Dams and Reservoirs under Changing Challenges – Schleiss & Boes (Eds)
© 2011 Taylor & Francis Group, London, ISBN 978-0-415-68267-1

Estimation of rockfill dam behavior during impounding by elasto-plastic model

N. Tomida, N. Sato, H. Soda & S. Jikan
Japan Water Agency, Saitama, Japan

K. Ohmori
Ridge Research Institute of Digital Geo-Environment, Kanazawa, Ishikawa, Japan

H. Ohta
Research and Development Initiative, Chuo University, Tokyo, Japan

ABSTRACT: Tokuyama dam is one of the largest rockfill dams in Japan, which JWA constructed across the Kiso River. Since width of the central core of Tokuyama dam was redesigned to be thinner than the original design. Therefore, evaluation of the safety of the core zone during the impounding period was carried out by both numerical analysis and observed data. In this report, following the actual construction process of embankment and impounding, an elasto-plastic soil/water coupled consolidation analysis is carried out to find the rise of pore water pressure and change of effective stress in the core zone. The safety level of the core zone during the impounding period was evaluated by Seed standard.

As a result, numerical analysis and observed data matched closely, which confirmed the validity of the analysis. The safety of the core zone during the impounding period was confirmed by both observed data and numerical analysis.

1 INTRODUCTION

Tokuyama dam is a multi-purpose dam constructed by JWA. It is one of the largest rockfill dams in Japan with the dam height of 161 m, the dam volume of 13,700,000 m^3 and the gross storage capacity of 660,000,000 m^3.

Figure 1 shows the location of Tokuyama dam. The construction work started in March, 2000, and completed in the end of November, 2005. The first impounding commenced on September 25, 2006. The water level in the reservoir reached surcharge water level on April 21, 2008, followed by the completion of the first impounding on May 5, 2008.

In Japan, the bottom width of the core zone of rockfill dams is normally around 40–50% (Ministry of Construction River division, 1987) of the dam height. The final design of Tokuyama dam applied thinner shape, and its bottom width of the core zone is 36% of the dam height. Due to adopting the thinner core zone than normal design, the stress reduction was concerned. So the appropriate estimation on safety against failure during the impounding period was necessary.

In this report, an elasto-plastic soil/water coupled consolidation analysis was carried out to simulate the physical behaviors within the dam body based on the actual construction process of embankment and impounding in Tokuyama dam. A comparison of the numerical analysis and observed data shows similarity, which proved the validity of elasto-plastic soil/water coupled consolidation analysis. The safety of the core zone during the impounding period was also estimated by using the results of this analysis.

Figure 1. Location of Tokuyama dam.

2 OUTLINE OF THE ANALYSIS

The analysis predicts the pore water pressure and minor principal stress of the core zone as the following procedures, in order to evaluate the safety level for hydraulic fracturing during the first impounding. Firstly, the rise and dissipation of pore water pressure of the core zone during the embankment is predicted. After that, the dam body behavior during impounding is analyzed in the initial conditions of the first impounding decided by the first prediction. During the impounding period, the elasto-plastic soil/water coupled consolidation analysis is carried out to estimate the rise of pore water pressure, the rise of osmotic pressure at the upper part of the dam body, the change of the effective stress and the dam body behavior. In the above analysis, the elasto-plastic soil/water coupled consolidation model is adapted as the model of the embankment material of dam.

The elasto-plastic soil/water coupled consolidation model employed a stress-distortion relationship (constitutive law) of Sekiguchi-Ohta model (Sekiguchi and Ohta, 1977) which can cover embankment material with anisotropy and predict the volume change of soil induced by compression stress and shear accurately. Figure 2 shows the conceptual diagram of elasto-plastic model. Table-1 shows main parameters used for analysis.

The analysis parameters of filter material and core material are set based on material test whereas that of rock material is based on both material test and observed data at site. The earth pressure coefficients at rest K_0 of each material is 0.7.

Figure 3 shows the relation between coefficient of permeability and void ratio of core material in Tokuyama dam. The coefficient of permeability of saturated soil obtained from consolidation test is 10 times larger than that of unsaturated soil obtained by consolidation test. The coefficient of permeability obtained from permeability test on embankment surface at site matches closely with that of saturated soil obtained by consolidation test. The coefficient of permeability used for the analysis is set based on the result of consolidation test of unsaturated soil, since the core material is unsaturated during embankment. The initial coefficient of permeability is obtained by consolidation test in which void ratio of the material was adjusted to the average void ratio in embankment area at site. Because the material of core with small void ratio tends to have lower permeability, coefficient of permeability is changed according to the change of void ratio obtained from the analysis, using the relationship between the coefficient of permeability and void ratio obtained from the consolidation test shown in dotted line in Figure 3. In the analysis, the coefficient of permeability is changed in every embankment stage.

Figure 4 shows the cross section of Tokuyama dam used for the analysis. Tokuyama Dam has the height of 161 m, upstream slope gradient of 1:3.0, downstream slope gradient of

A-B:Elastic territory
(Embankment load < Compaction by the pre-compression stress Pc)

B-C:Elasto-plastic territory
(Embankment load ≥ Compaction by the pre-compression stress Pc)

C-D:Elastic territory
(Decrease of the effective stress by the impound)

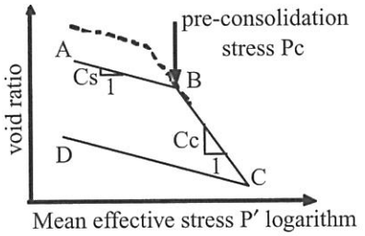

Figure 2. Conceptual diagram for elasto-plastic model.

Table 1. Material parameter for the analysis.

Category	Unit	Rock material	Filter material	Core material
Swell index (Cs)		0.0375	0.0033	0.0045
Compression index (Cc)		0.0860	0.0140	0.0215
Pre-consolidation stress (Pc)	(kPa)	820	920	132
Friction angle (ϕ')	(degree)	43.3	39.4	37.8
Coefficient of permeability	cm/sec	3.05×10^{-1}	8.0×10^{-4}	1.93×10^{-7}
Critical state parameter (M)		1.78	1.61	1.54
Irreversiblity ratio (Λ)		0.564	0.764	0.791
Coefficient of dilatancy (D)		0.00317	0.00234	0.00928
Effective poisson ratio (ν')		0.412	0.412	0.412

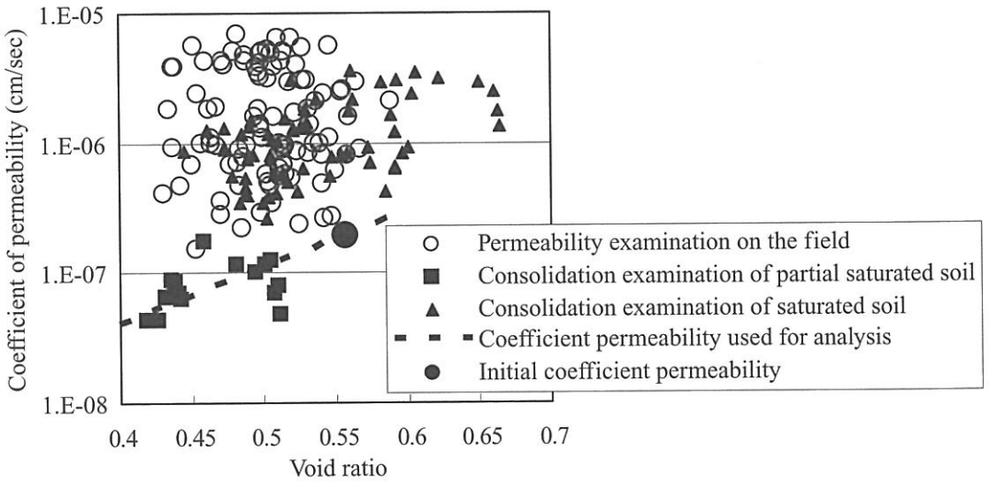

Figure 3. Relation between core material's coefficient permeability and void ratio.

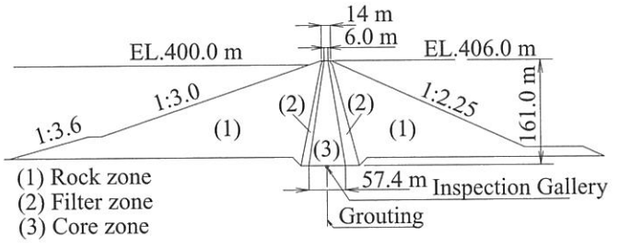

Figure 4. Cross-section.

1:2.25, and its symmetric core slope has a gradient of 1:0.16. The analysis is implemented for the dam body and the foundation. The analysis horizontal range is about the double of the base width and the vertical range is about the double of the dam height. The number of elements is 5524 in the finite elements method. As the boundary conditions, the horizontal displacement at the side of the foundation is 0 and that at the underside is fixed. As the hydraulic boundary conditions, the distribution load and hydrostatic pressure based on the reservoir level is set on the upper face of the dam. Also the vertical load based on the difference between the wet density and saturated density is set at the dam body under water. The pore water pressure at the lower rock zone is set as 0 during the embankment and impounding period. As the boundary conditions, the water pressure based on the reservoir level at the upper side of the foundation, the hydrostatic pressure at the lower side of the foundation and the undrained condition at the underside are set respectively.

In the embankment analysis, in order to represent the actual embankment process, the elements of dam body are accumulated successively based on the embankment process as shown in Figure 5.

In the impounding analysis, the effective stress is numerically predicted by an unsteady-state seepage analysis in saturated soils with a time dependent boundary condition of escalating water level in reservoir.

The fracturing pressure of the core zone is evaluated by "(Seed and Duncan, 1981)". Seed suggests a quantitative evaluation method of hydraulic fracturing which defines the condition of soil destruction with crack by the following formula.

$$u_f = \sigma_3 + \sigma_t \tag{1}$$

where u_f = hydraulic fracturing pressure; σ_3 = minor principal stress in total stress; σ_t = tensile strength of soil.

In this report, the generation of hydraulic fracturing of core material is based on the Seed standard. Local safety factor against hydraulic fracturing (Fsh), is obtained by formula (2), neglecting tensile strength of soil to evaluate in a severer condition.

$$Fsh = (\sigma_3 + \sigma_t)/\Delta u \tag{2}$$

where Δu = pore water pressure.

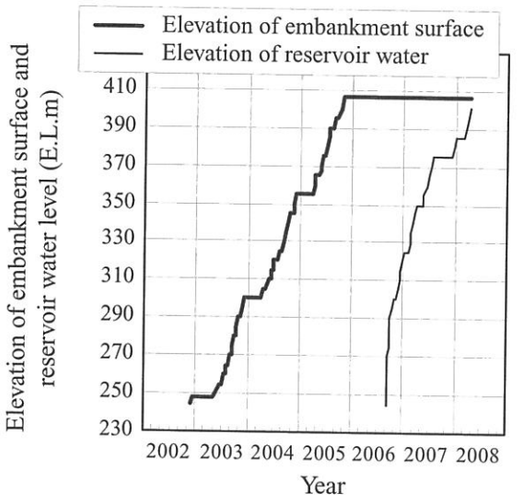

Figure 5. The process of embankment and impounding turned into a model by FEM analysis.

3 INVESTIGATION AND CONSIDERATION ON RESULT OF DAM BODY BEHAVIOR ANALYSIS COMPARED WITH ACTUAL VALUE

Figure 6 shows the comparison of settlement value at the same location between numerical result and data measured by settlement gauge A-2. The comparison shows close similarity when the water level reaches the maximum water level.

Figure 7 and Figure 8 show another comparison at the same location between numerical results and data measured by vertical earth pressure gauge, E-14 set up in the upper side of middle elevation of core zone and E-15 set up in the center part. The comparison of the value at E-14 between numerical results and data measured at site shows a close similarity, whereas that of E-15 does not. At E-15, earth pressure is numerically predicted larger by 30% than observed data.

Figure 9 and Figure 10 show a comparison of pore water pressure between numerical results and measured data at the time of maximum water level during the first impounding.

Residual pore water pressure exists after the completion of embankment, but the osmotic pressure in the core rises due to the impounding. Both observed data and numerical prediction show the dissipation of pore water pressure when the water level reaches the maximum water level, leaving the profile of pore water pressure high at the upper stream and low at the downstream.

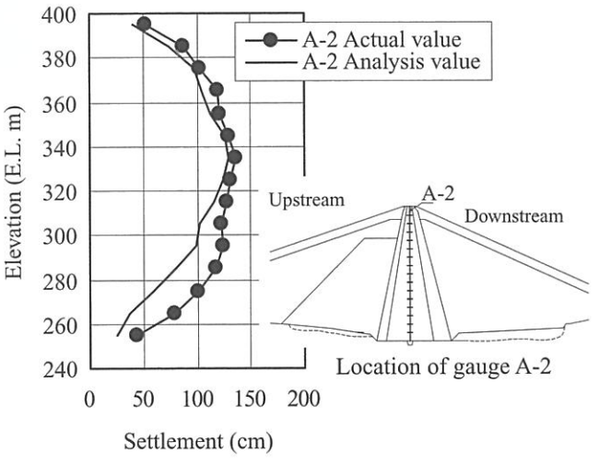

Figure 6. Actual value and analysis value by differential settlement gauge (Maximum water level).

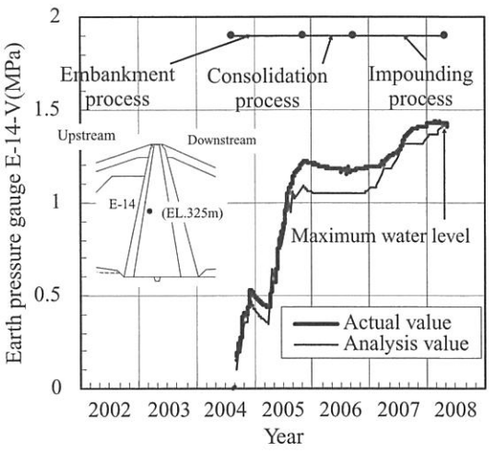

Figure 7. Chronological change of Vertical Earth Pressure.

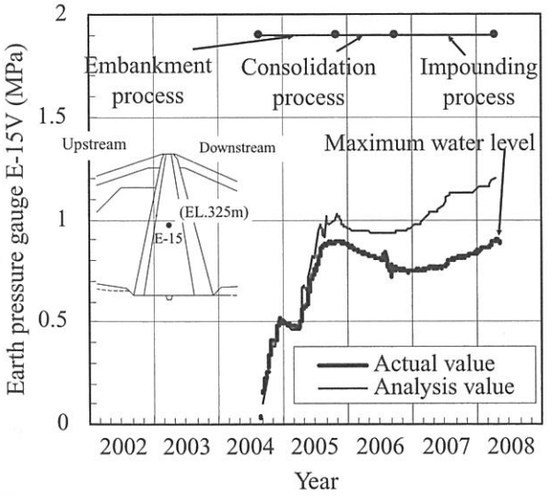

Figure 8. Chronological change of Vertical Earth Pressure.

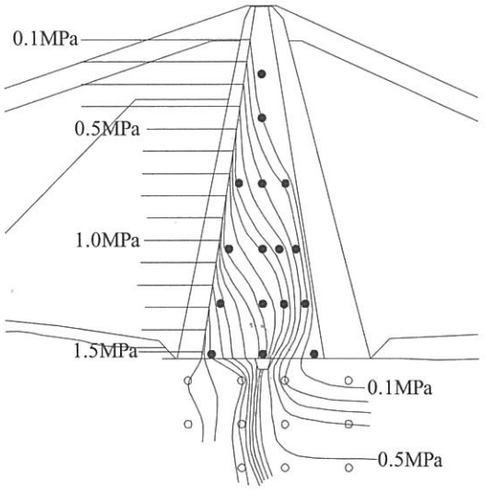

Figure 9. Distribution map of Pore water pressure on highest high-water level (actual value).

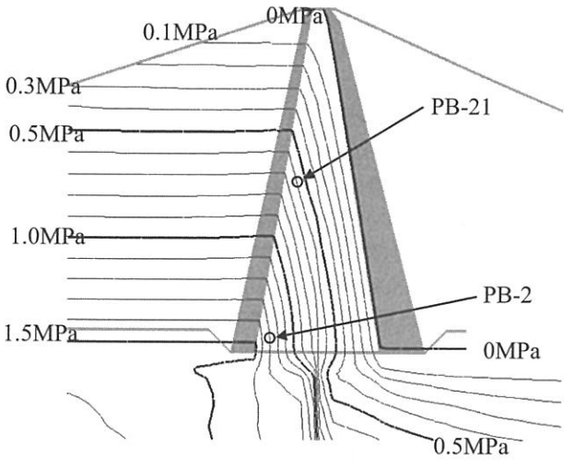

Figure 10. Distribution map of Pore water pressure on highest high-water level (analysis value).

Figure 11 and Figure 12 show a comparison of pore pressure at the same location between numerical prediction and observed data measured by pore pressure gauge at PB-21 set up in the upper side of middle elevation of core zone and PB-2 set up in the lower elevation. It shows similarity between numerical result and observed data of pore water pressure during the process of embankment and at the time of the maximum water level. Differences between numerical prediction and observed data are seen from November, 2005 to March, 2007. During this term, observed data tends to be larger than numerical prediction. The dissipation of water pressure is calculated by seepage analysis, on the assumption that the core is saturation. On the other hand, the core is unsaturated during this term, so the coefficient of permeability is small, seemingly resulted in the delay of dissipation of pore water pressure.

Figure 13 shows distribution contour of major effective principal stress at the end of embankment obtained by the embankment analysis. The generation of arching phenomena due to the difference of rigidity between core zone and filter zone leads the stress reduction in the core zone.

Figure 14 shows a comparison of the major principal stress σ_1, minor principal stress σ_3 and pore water pressure at the same location between numerical prediction and data measured at E-14. Observed major principal stress σ_1 and minor principal stress σ_3 are calculated based on the data from trihedral earth pressure gauge. The numerical prediction is successful to simulate the qualitative trend of pore water pressure inside of the core, major principal stress in total stress σ_1 and the minor principal stress in total stress σ_3, to increase parallel with the water level in the reservoir. Observed data and numerical prediction of minor principal stress σ_3 shows a close similarity. In addition to that, major principal stress in total stress σ_1 and minor principal stress in total stress σ_3 surpass pore water pressure in every point.

4 CONSIDERATION ON THE SAFETY AGAINST THE HYDRAULIC FRACTURING

Figure 15 shows the distribution contour of safety factor against hydraulic fracturing at the core zone obtained by the analysis at the time of the maximum water level. The safety factor against hydraulic fracturing becomes the smallest at the border of the core zone and the filter zone at the height of 1/3–2/3 of the dam height. The smallest safety factor is approximately 1.3.

On the other hand, Figure 16 shows both the safety factor against hydraulic fracturing in the core zone obtained from the observed data and that from the analysis. The smallest safety factor obtained by the observed data is 1.56, and that of numerical prediction is 1.42. Although observed data is a little larger than numerical prediction, safety factors in the core zone are nearly equal.

From these points, smallest safety factor against hydraulic fracturing at the core zone in Tokuyama dam is 1.56 based on observed value and 1.4 from numerical prediction, which confirms "safety factor ≥1.0" in every point.

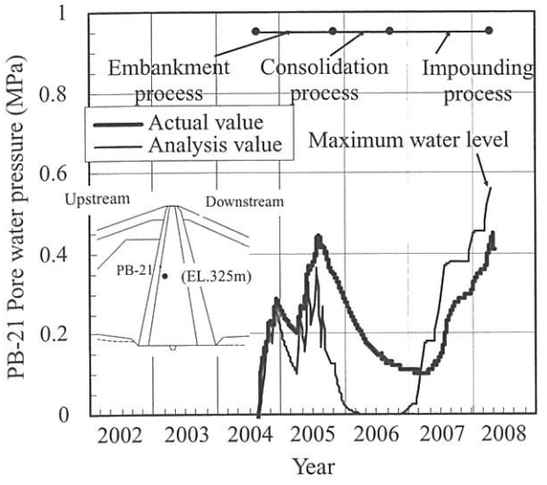

Figure 11. Chronological change of pore water pressure.

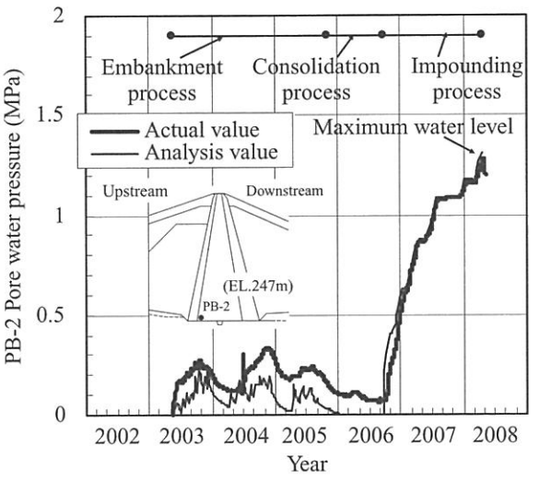

Figure 12. Chronological change of pore water pressure.

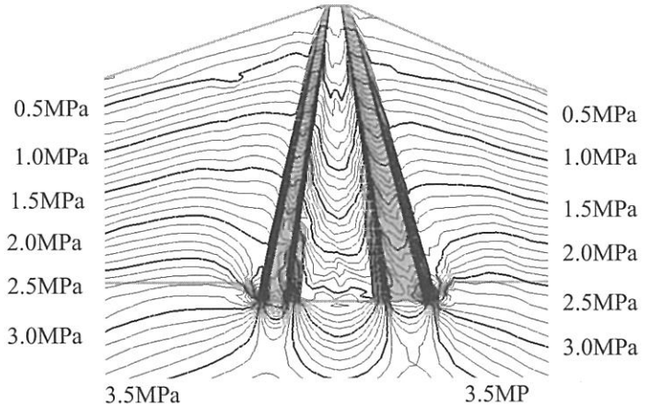

Figure 13. Distribution map of major effective principal stress when the embankment was completed (analysis value).

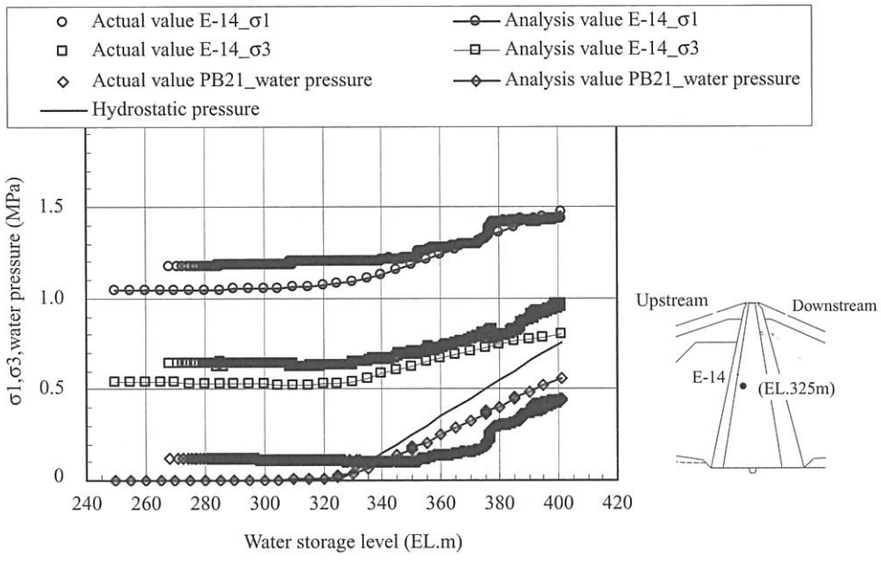

Figure 14. Chronological change of major, minor principal stress and Pore water pressure on E-14.

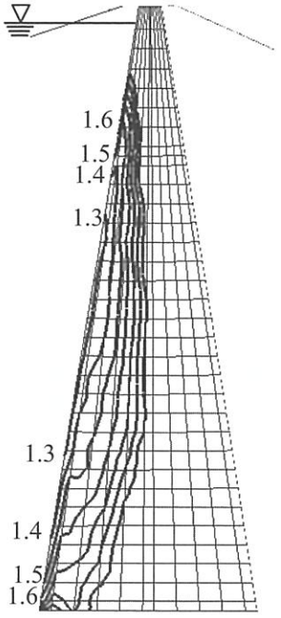

Figure 15. Distribution contour of safety factor against hydraulic fracturing in the core when the water level reached maximum water level (analysis value).

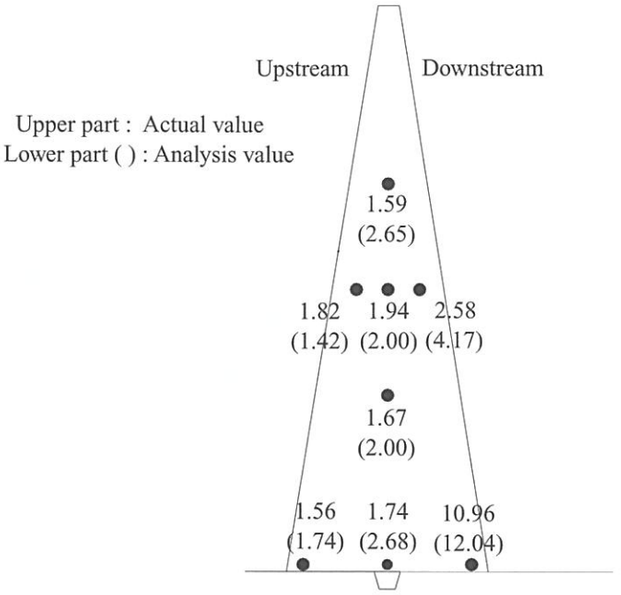

Figure 16. Safety rate against hydraulic fracturing of central core.

5 CONCLUSION

In this report, the numerical prediction of dam body behavior based on actual construction process of embankment and impounding in Tokuyama Dam is implemented by using elasto-plastic soil/water coupled consolidation analysis which can cover the rise and dissipation of pore water pressure and rise of osmotic pressure. As a result, the numerical prediction of settlement and vertical earth pressure from embankment to impounding are similar to that of observed data. The numerical prediction of pore water pressure is similar to that of observed data during the process of embankment and when impounding is completed. The numerical prediction is successful to simulate the qualitative trend of pore water pressure, major principal stress and minor principal stress in the core zone to increase parallel with the water level in the reservoir.

From these points, numerical prediction of dam body behavior in Tokuyama Dam is successful to prove the validity of elasto-plastic soil/water coupled consolidation analysis. The smallest safety factors against hydraulic fracturing at core zone in Tokuyama Dam are approximately 1.56 based on observed data and 1.4 based on numerical prediction. Safety against hydraulic fracturing is also confirmed since the smallest safety factors surpass 1.0 in both values.

Observed data during the first impounding did not show any abnormal phenomena in permeability and deformation of dam. The results of the numerical prediction matched with those observed data.

REFERENCES

Ministry of Construction River division (Supervisor), 1987, Constructions of multi-purpose dam, 4th volume: 84. Tokyo: Dam Engineering Center foundation (in Japanese).

Seed, B. & Duncan, J.M. 1981. The Teton Dam Failure- A Retrospective Review, Proc. of 10th ICSMFE: 1–20.

Sekiguchi, H. & Ohta, H. 1977. Induced anisotropy and time dependency in clays, Proc. of 9th ICSMFE: 229–239.